Single hole direct injector simulation validation and parametric sensitivity study

Single hole direct injector simulation validation and parametric sensitivity study

Mohamad Hafidzul Rahman Alias[1], **Mohd Fadzil Abdul Rahim**[1,2,*] **and Rosli Abu Bakar**[1]

[1] Faculty of Mechanical Engineering, Universiti Malaysia Pahang, Pahang, Malaysia.
[2] Innovative Manufacturing and Mechatronics and Sports (IMAMS) Laboratory, Faculty of Manufacturing Engineering, Universiti Malaysia Pahang, Pahang, Malaysia.

*Corresponding author: mfadzil@ump.edu.my

Abstract. This paper presents a parametric study conducted on electronically controlled solenoid direct fuel injector running on compressed natural gas. The purpose of the study is to identify the influential injector parameters on the output fuel mass flow rate. These injector parameters are to be optimize in the next stage of the study. The parametric study is conducted using zero-dimensional, first principle injector model which consist of electro-magnetic, mechanical and flow sub-models. In current study, seven (six input and one output) selected parameters have been analysed which are the injection pressure, injection duration, nozzle diameter, armature mass, the input voltage, spring constant and the output mass flow rate. Each input parameters are varied in the prescribed range based on the literature. Based on the study, the most influential parameters (in rank) are the nozzle diameter, the armature mass and the injection duration. The input voltage, the injection pressure and the spring constant were found to have no impact on the injector mass flow rate based on the values of parameter's sensitivities. Based on the results, the potential parameters to be optimized are identified.

Keywords. Compressed Natural Gas; Direct injection; Modelling; Parametric study

1. Introduction

For many years, researchers and manufactures have been working hard to comply with the ever demanding stringent emissions regulations set by every country around the world. Compress natural gas (CNG) has already regarded as one of the most recognize fuel for Gasoline and Diesel replacement. Compared to conventional fuel, the fuel cost of CNG is 20 to 40% lower which is the major advantage [1]. CNG also mostly sought after for the sake of its massive reserves and its distinctive cleaner combustion [2].

Set against the conventional fuels, CNG has a higher thermal efficiency and higher knock resistance [3], [4] as a result of its high octane number (RON = 110–130).[5], [6] Furthermore, thanks to its peculiar ratio between carbon and hydrogen CNG fuel can produce a much higher compression rate while emits a far less CO2 compare conventional fuels.[5], [6] Basically, a natural gas engines can be conducted at lean burn under stoichiometric circumstances and will promote a diversity of combustion and emission qualities [7].

Port-injected CNG technology has been put into trials phase, sadly market still prefer the conventional fuelled vehicles better. The reason behind it was refuelling stations insufficiency and when compared to gasoline, the power and torque produced were relatively lower [4]. Port-injected engines generally known to work in stoichiometric mixture of air fuel ratio (AFR) complementary to its mode combustion of homogeneous-charge [8].

Meanwhile, in rotary engine the most prominent problem when using CNG as the fuel is the inadequate fuel combustion process, in which it can surpass the typical utilization of fuel as well as give out a much higher emissions than before. Installing the turbocharger is one of the many ways to better refining the commercial grade and emission waste of rotary engine.[9] Diesel engine is a more utilized platform for CNG engine conversion [10]. A comparison study between direct injected gasoline, port injected gasoline and carburetted gasoline have been conducted.[11] A crucial information obtained from the results where it is found that the maximum power of CNG-DI is only 5% lower than gasoline port injection.

The scientific and technical knowledge behind the technology of Direct Injection (DI) system can be the solution to resolve the spark-ignition engines performance when using natural gas as fuel. DI system give the engine a boost in its volumetric capability [2], [8] which allows an increasing in total power hence give the engine what it take to drive at more advance velocity pace. Along with that, DI will reduce the needed for throttling control[6], to such a degree the pumping revolution deficiency and heat transfer losses can be cut down which promote low fuel consumption[7].

It is concluded that CNG-DI engine has the best capability to revamp fuel flow and ignition process that stimulate a more comprehensive engine performance and lessen the fuel usage [11] as well as emissions.[5], [8] As the DI system enhancing the injection strategy and carry out the stratified allocation of fuel, it is able to accurately manage the framework of fuel injection, such as injection timing and the angle of injection [9]. The latest Gasoline direct injection (GDI) system can be operate at 80 to 200 bar of pressure based upon its operating setting [8]. GDI engines can run on homogeneous stoichiometric combustion mode as well as the advanced combustion mode of stratified-charge [8].

Per contra, the technology of DI system as it may be constructive features it is also has the destructive consequences upon the engine. In the homogeneous-charge combustion mode, the spray-induced flow might increase the instability in cylinder chamber. The uniformities of fuel blend can be deteriorated because of the reduction in time period and gap area of air fuel mixture. In the stratified-charge combustion mode, in order to have a better controllability of fuel injection, the DI is required to introduce a very high pressure to the fuel injection operation which is evidently a complex task to solve because of the leaking issue of CNG happen around the nozzle area [2].

Nearly all conventional fuel injectors are solenoid drive unit. The electrical energy transmitted to the injector will magnetized and demagnetized solenoid in the injector which is then translated into mechanical energy. The mechanical energy is define by the movement of needle in the injector as it open and close which control the fuel flow through the nozzle. The needle movement are called injector temporal characteristics. These temporal characteristics of an injector such as injection duration, injection frequency, rate shape, opening delay time and closing delay time are controlled by the engine control unit (ECU). A predefined optimal setting stored in the base maps of the ECU and will send the control signal to the power driver of fuel injector.

The challenge for CNG is as there is neither dedicated CNG direct injector nor commercialize direct injector for gaseous fuel. Hence, we resorted to conversion of conventional direct injector. The changes of fuel properties from liquid to gases affect the injector characteristic benchmarked by the manufacturer. This is why the injector characterization for the natural gas engine is greatly desired by researchers. There are also already have been an adaptation of bi-fuel system into the conventional gasoline engine where gasoline and CNG will be use as the fuel but the attempt on this system proven to be not as reliable it were thought. This system is lack of brake power and generates way more emissions than conventional engine. Most of the engine that converted into the bi-fuel system is initially were multiport injection (MPI) oriented, where the engine are known to be unable to produce high thermal capacity [11].

Based on the literature review, from the previous studies on direct fuel injector we know that CNG is a low cost fuel, have a large reserve, and contribute to a low emissions from it cleaner combustion process. CNG have been implemented in various engine categories, such as port injection engine, direct injection engine, diesel engine even rotary engine. Direct injection has been identified as the most relevant option to improve natural gas engine performance. However, injection characterization study were basically conventional fuel application oriented mainly focus on diesel and gasoline. Hardly any study of direct fuel injector characterization for natural gas can be found. Therefore, it is very crucial to investigate the injection characteristics of CNG direct injection as it affects the overall engine performance.

This study was conducted to specifically investigate the most influential injector parameters on the output fuel mass flow rate using CNG as the fuel. A parametric study has been conducted on electronically controlled solenoid direct fuel injector for it to be running on CNG. For this parametric study, it will be conducted using zero-dimensional, first principle injector model which consist of electro-magnetic, mechanical and flow sub-models. The selected input parameters have been analysed which are the injection pressure, injection duration, nozzle diameter, armature mass, the input voltage, spring constant and mass flow rate as the output parameter. Each input parameters are varied in the prescribed range based on the literature. For the next stage of the study, these selected injector parameters will going to be optimized. Finally, this study is hoped to bring a better understanding of cause-effect relationship among injector parameters.

2. Methodology (simulation model equation)

The modelling section is divided into three different section; the electromagnetic model, the mechanical model and the flow model. These models are combined and developed in MATLAB Simulink software. The Matlab ODE solver is selected as the baseline solver in the study.

2.1. The electromagnetic model

The electromagnetic is based on the work of Schimpf [12]. The solenoid driver presented by Schimpf is a derivation of electromagnetic force regarding coil diameter, coil length, wire gauge, supply voltage, packing density, and the number of turns. This model eliminates the current term which in most cases are difficult to solve. Detail discussion and explanation of the model can be found in Schimpf. The electromagnetic force is given by the following expressions:

$$F_{mag} = \frac{V^2 u_r u_0}{8\gamma^2 l^2} \left(\frac{r_0}{r_a}\right)^2 \alpha e^{-\frac{\alpha}{l}x} \tag{1}$$

or

$$F_{mag} = \frac{V^2 u_r u_0}{8\gamma^2 l^2} W_f \alpha e^{-\frac{\alpha}{l}x} \tag{2}$$

Where;

V : Supply voltage
u_r : Relative magnetic permeability of armature/pintle material
u_0 : Air gaps magnetic permeability
r_0 : Inner radius of coil cross section
r_a : Average radius of coil cross section
γ : Ratio of coil material resistivity to coil wire cross section area
W_f : Winding factor, equal to square of $\frac{r_0}{r_a}$ ratio
l : Length of coil body
a : Ratio of inductance to relative permeability of armature material
x : Instantaneous position of armature

To utilize the model, one needed to have detail information of the coil material. For example, the type of coil material, coil material resistivity and coil wire cross-section area. In general, the larger the coil wire cross section area, the larger the generated force. In the study, the selected coil wire is estimated to be based on AWG 43 which has a diameter of 0.07874 mm and copper type.

2.2. The mechanical model

The mechanical system of the direct injector is represented by a mass-spring-damper system. In the initial state, it was assumed that the pintle sits on the valve seats. In this initial state, a total of five forces are acting on the pintle. The gas pressure force, contact friction force, gravitational force, initial spring force, and finally normal reaction force**.** Figure 1 presents the free body diagram of the pintle in the study. The gas force is due to the CNG fuel pressure, the contact friction force is due to the contact between the pintle and surface of the valve seats, and the gravitational force is due to the mass of the pintle. The initial spring force is due to the compression of the spring at the initial state. Additional spring force will be generated as the pintle is pulled by the solenoids. The normal reaction force defines the existence of the lower and upper stopper of valve seats. This force is represented by the virtual spring, and damper unit which is equal and opposite direction of all other forces when the pintle rest or hit bottom and upper stopper.

The pintle act as a plunger which controls the open and close the nozzle flow area. During the opening state of the injector, the pintle will overcome all the resistant forces by withdrawing required current from the power supplies. The relationship between the all the forces is described by the mathematical expressions of the pintle's equation of motion which is given by equation (3). Based on the equation, the displacement of the pintle can be obtained by a twice integration of the acceleration. The mass considered in the equation is only the mass of moving the rigid body of the pintle.

$$m.\ddot{x} = F_{sol} + F_{spring} + F_{contact\ friction} + F_{upper\ wall} + F_{bottom\ wall} + F_{pressure} \quad (3)$$

The spring compression force F_{spring} is defined as the sum of initial compression force and the force due to the additional compression during the solenoid activation. The equation for the spring compression force is given by the following expression.

$$F_{spring}(x) = F_0 + K_{spring}.x \quad (4)$$

Where;

F_0 : The initial compression force, N
K_{spring} : Spring constant, N/m

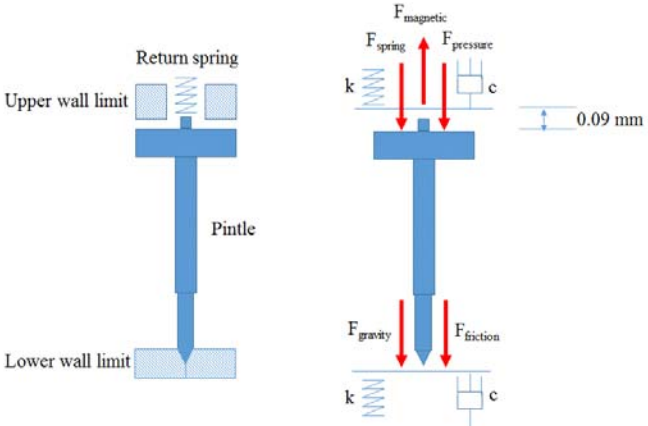

Figure 1. Pintle free body diagram[13].

The initial contact friction force is given a constant value of 13.8 N at its rest position (at the upper stator or lower stator). The value will reduce to zero as the position of the pintle surpassed a threshold distance of 0.001 mm. The mathematical form of the contact friction force is given by equation (5).

$$F_{initial\ contact\ friction}(x) = \begin{cases} -13.8\text{N}, and\ x \leq 1e-3mm \\ 0, and\ x > 1e-3\ mm \end{cases} \quad (5)$$

Based on the findings of Zhang et al.[14], the displacement of the pintle is limited by the existing of the bottom and upper stator. The maximum displacement allowable for the pintle is estimated to be 0.09 mm upwardly. Farther than that, a barrier is enforced by imposing a stiff spring and damper. This is to simulate a condition where the pintle hits the stator. The reaction force imposed on the pintle at the upper wall is expressed mathematically by equation (6).

$$F_{upperwall}(x) = \begin{cases} -K*(x0.09mm) - c*x, and\ \dot{x} < 0 \\ 0, and\ x > 0 \end{cases} \quad (6)$$

As the pintle moves back to the initial position and hit the lower stator, another barrier is imposed to simulate the reaction force from the bottom stator. The mathematical expression for the lower stator reaction force is given by equation (7).

$$F_{bottom\ wall}(x) = \begin{cases} -K^* - C^*x, and\ \dot{x} < 0 \\ 0, and\ x > 0 \end{cases} \quad (7)$$

Where;
K : the wall stiffness, N/m
C : the damping coefficient, N·s/m

2.3. The flow model

The flow model is based on one-dimensional compressible flow equation. The model considers choking and non-choke flow situations which are determined by the critical pressure ratio. Choked flow occurs when the ratio P_1/P_2 exceeds the critical pressure ratio P_c, which is given by the following equation.

$$P_C = \left(\frac{\gamma+1}{2}\right)^{\frac{\gamma}{(\gamma-1)}} \quad (8)$$

The mass flow rate through the orifice for non-choked and choked flow conditions are given by equation (9) and (10) respectively. The only varying parameter in the equation (9) is the effective area of the nozzle which is calculated as a function of pintle displacement.

$$\dot{m} = K_{nv}AP_1\sqrt{\frac{2M}{RT}\left(\frac{\gamma}{\gamma-1}\right)\left[\left(\frac{P_2}{P_1}\right)^{\frac{2}{\gamma}} - \left(\frac{P_2}{P_1}\right)^{\frac{\gamma+1}{\gamma}}\right]} \quad (9)$$

Or

$$\dot{m} = K_{nv}AP_1\sqrt{\frac{\gamma M}{RT}\left(\frac{2\gamma}{\gamma-1}\right)^{\frac{\gamma+1}{\gamma-1}}} \quad (10)$$

Where;

K_{nv} : The discharge flow coefficients
A : The orifice area (m^2)
P_1 : The H^2 upstream pressure (Pa)
P_2 : The in-cylinder pressure (Pa)
T : The H^2 upstream temperature (K)

The crucial part of the flow model is the definition of the nozzle effective flow area. Figure 2 presents a schematic definition of the nozzle effective flow area for the pulled-in injector. The effective flow area is defined as a surface area of a truncated cone. The effective flow area is formulated based on the work of Antunes.[15]

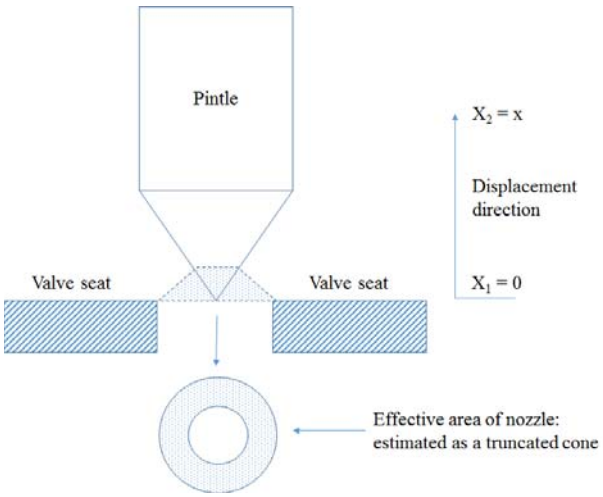

Figure 2. Definitions of effective flow area for nozzle flow calculation[15].

In mathematical form, the effective area for the nozzle flow, as illustrated in figure 2, can be calculated by using equation (11).

$$A_O = \pi \left[\frac{\left(R\sqrt{R^2 + (R\,sin\varphi)}\right) - (R - X\,sin\varphi sin\varphi)}{\sqrt{(R - X\,sin\varphi sin\varphi)^2 + (R\,tan\varphi - X sin^2\varphi)^2}} \right] \quad (11)$$

Where;

R : The nozzle hole radius (m)
θ : The needle tip angle (rad)
$\emptyset$: Equal to $\theta/2$

The maximum area of the nozzle is given by:

$$A_{O\,Max} = \pi R^2 \quad (12)$$

3. Simulation model setup

The simulation was carried out to replicate the two cases from the experiment for validation. A significant amount of inputs are required to ensure the model can predict as close as possible to the measured data. Table 1 is the general specification for the injector to make sure the simulation model is not out of the course while table 2 listed all the general and specific inputs required by the model. The electro-magnetic inputs, as well as the mechanical inputs parameter of the injector, are mostly based on Zhang et al.[14]. Figure 3 presents the schematic layout of the experimental work which is use as a reference to develop the layout of the simulation model in MATLAB Simulink shows by figure 4. The pulse generator produced square wave signal which represents the output of the PWM driver.

Table 1. General BOSCH Model HDEV 1.2 injector specification[16].

Attributes	Values
Mechanical specifications	
Allowable maximum pressure (bar)	200
Volume flow rate (gasoline fuel/cm3/min) at 100 bar	30
Weight (g)	78
Length (mm)	85
Electrical specifications	
Resistance (Ohm)	0.9 @ 1.5
Voltage (Volt)	90 V
Allowable peak current (Amp)	20 A
Operating Condition (Gasoline fuel)	
Fuel Input	Axial (top feed)
Operating Temperatures (°C)	30-120
Permissible Fuel Temperatures (°C)	<80

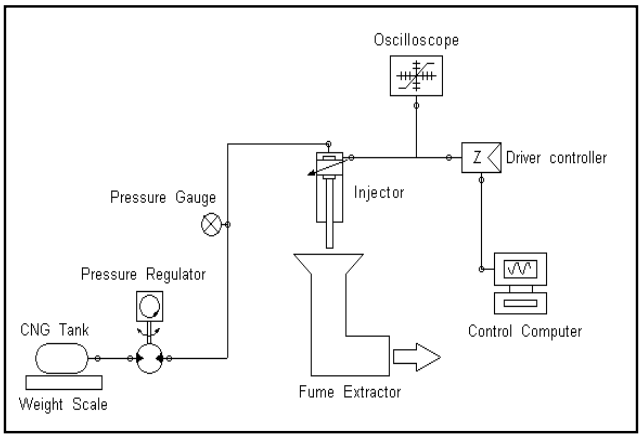

Figure 3. Schematic diagram of experimental setup.

Table 2. Simulation model input.

Attributes	Values
General Input Parameter (unit)	
Actuator radius (m)	0.005
Gas pressure (bar)	50
Nozzle Diameter(m)	0.00068
Spring Constant (N/m)	12140 N/m
Electro-magnetic Input Parameters (unit)	
Length of air gap (m)	0.00009
Magnetic Permeability of Air (H/m)	1.256×10^{-6}
Magnetic Permeability of Steel (H/m)	3290
Magnetic circuit length (m)	~0.001
Number of Turns	160
Coil Resistance (Ohm)	0.9
Resistance (ohm)	1.5 (Zhang)[14]
Inductance (mH)	1.9 mH @ 1kHz 3.9 mH @0.12 kHz
Voltage (Volt)	90
Peak Current (Amps)	20
Mechanical Input Parameters (unit)	
Static Spring Force (N)	40
Spring mass (kg)	0.001
Actuator Mass (kg)	0.003
Actuator Damping Constant (Nm/s^2)	14.97 N.s/m
Overall Weight (kg)	0.078
Flow Input Parameters (unit)	
Gas specific heat ratio	1.32
Gas valve flow co-efficient	0.65
Universal gas constant (J/kg.K)	8314
Gas Molecular Mass (kg/kmol)	16.04
Gas Supply Temperature (K)	300

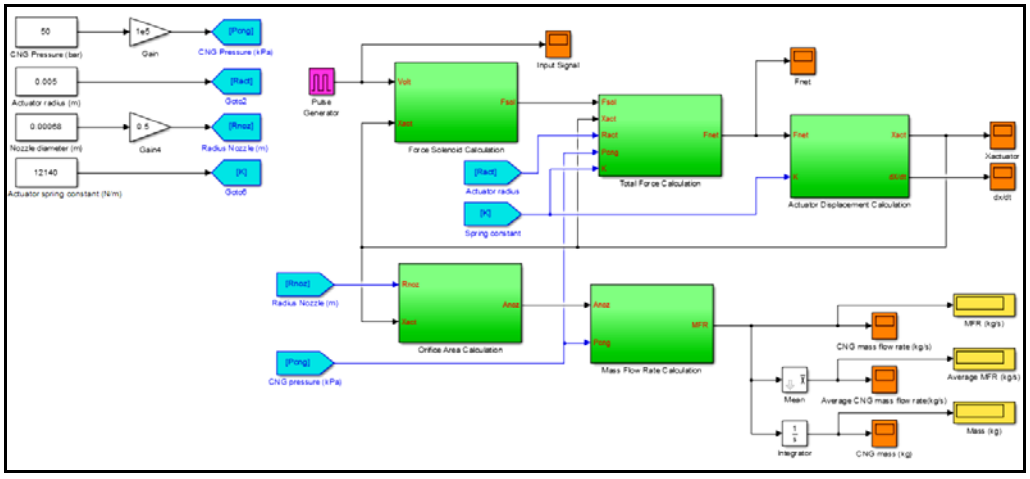

Figure 4. MATLAB Simulink block diagrams of the injector simulation model.

4. Results and discussion

4.1. Validation of simulation model (injection pressure)

Figure 5 shows the tabulation data between experiment and simulation result. The mass flow rate was measured at the injection pressure of 20 bar, 30 bar, 40 bar, 50bar and 60 bar for both experiment and simulation result. Based on the graph, both experiment and simulation result shows a linearly increasing trendline. It is proven that simulation result follow the experimental result trend. Thus, the simulated result therefore is valid for reference. There are just a small differences margin between the simulation and experiment result. The highest different mass flow rate between experiment and simulation is at 30bar at 52%. As a summary, simulation model can predict the expected result.

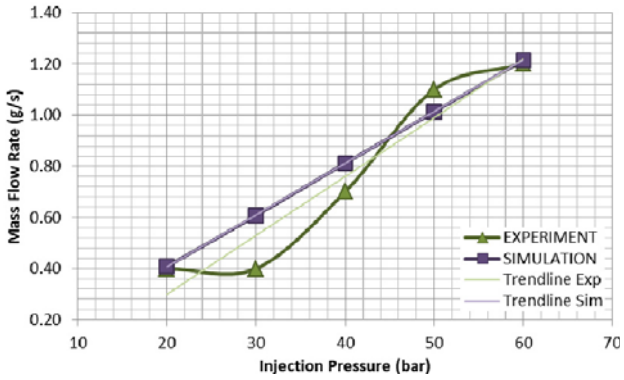

Figure 5. Comparison between experiment and simulation injection pressure.

4.2. Validation of simulation model (injection duration)

Figure 6 shows the tabulation data between experiment and simulation result. The mass flow rate for experiment and simulation result was measured at the injection duration of 2 ms to 24 ms with the increment of 2 ms for each injection duration increments. Based on the graph, both experiment and simulation result shows a linearly decreasing trendline. . Thus, it is proven that simulation result follow the experimental result trend. There are moderate differences margin between the simulation and experiment result. Although the simulated results have a moderate differences margin between experiment result, it is still valid for reference. The highest different mass flow rate between

experiment and simulation is at 4ms at 117%. As a summary, simulation model can only predict the trend at moderate accuracy.

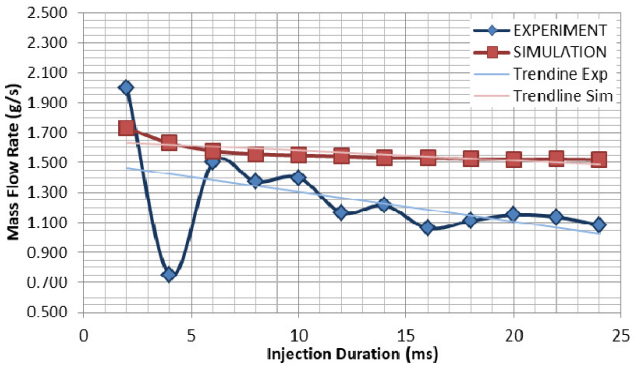

Figure 6. Comparison between experiment and simulation injection duration.

4.3. Parametric study of input voltage

Figure 7 shows the simulation result of input voltage versus mass flow rate. The mass flow rate for simulation result was measured at the voltage value of 6 V, 12 V, 24 V, 48 V and 90 V. Based on the graph, the simulated data show a linearly increasing trendline. Therefore, an increasing in the input voltage will directly affect the mass flow rate of the injector. The higher the input voltage is, the longer time it takes for the signal to turn off the armature. Thus, there will be more gas flow through the injector nozzle. As a summary, if the input voltage increases, then mass flow rate will also increase.

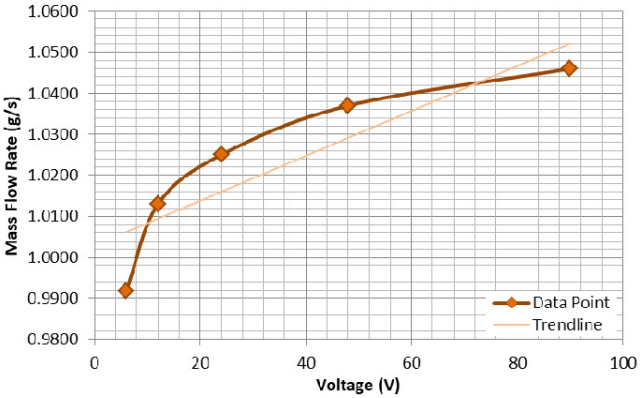

Figure 7. Simulation result of input voltage versus mass flow rate.

4.4. Parametric study of spring constant

Figure 8 shows the simulation result of spring constant versus mass flow rate. The mass flow rate for simulation result was measured at the spring constant value of 12000 N/m, 16000 N/m, 20000 N/m and 25000 N/m. Based on the graph, the simulated data show a linear trendline. Therefore, an increasing in spring constant value will not affect the mass flow rate of the injector. Spring stiffness only affect the opening and closing time of armature but not needle lift height. To add up, spring stiffness also affects a tiniest bit of the opening and closing time of armature making it insignificant. Thus, the mass flow rate for the injector will remain the same. As a summary, if spring constant increases, then mass flow rate will remain the same value.

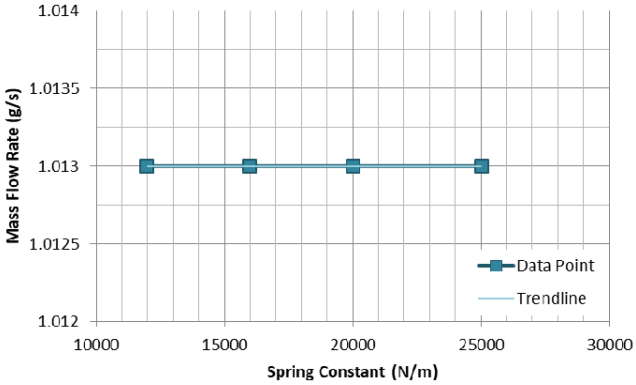

Figure 8. Simulation result of spring constant versus mass flow rate.

4.5. Parametric study of nozzle diameter

Figure 9 shows the simulation result of nozzle diameter versus mass flow rate. The mass flow rate for simulation result was measured at the nozzle diameter size of 0.0001 m, 0.0003 m, 0.0007 m and 0.0010 m. Based on the graph, the simulated data show a linearly increasing trendline. Therefore, an increasing in nozzle diameter size will directly affect the mass flow rate of the injector. A larger nozzle diameter size gives more space for gas to flow through the nozzle hence increases the mass flow rate of the injector. As a summary, if the nozzle diameter size increases, then mass flow rate will also increase.

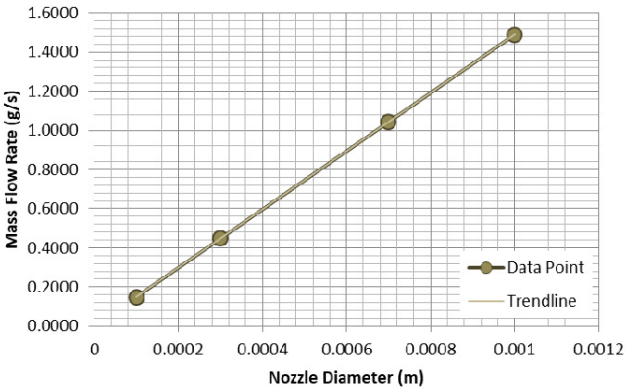

Figure 9. Simulation result of nozzle diameter versus mass flow rate.

4.6. Parameter study of armature mass

Figure 10 shows the simulation result of armature mass versus mass flow rate. The mass flow rate for simulation result was measured at the nozzle diameter size of 0.001 kg, 0.003 kg, 0.007 kg and 0.010 kg. Based on the graph, the simulated data show a linearly increasing trendline. Therefore, an increasing in armature mass will directly affect the mass flow rate of the injector. The heavier armature mass is, the longer time it takes for the spring to overcome the force. Thus, it provides a longer time for the gas to flow through the injector nozzle. As a summary, if armature mass increases, then mass flow rate will also increase.

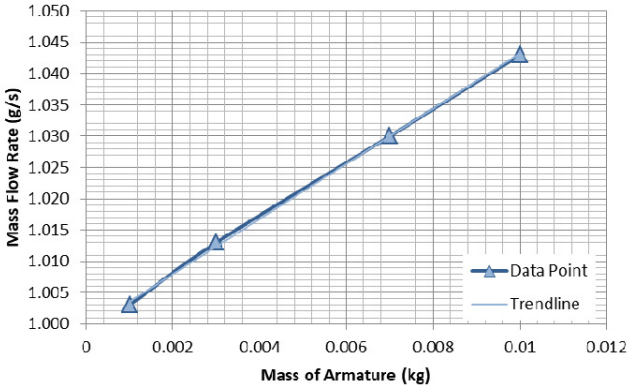

Figure 10. Simulation result of armature mass versus mass flow rate.

4.7. Parametric sensitivity ranking

Table 3 shows the sensitivity result of each parameter thus its ranking of sensitivity. Nozzle Diameter has the highest sensitivity with the value of 1489.705 g/s/m while Spring Constant has the lowest sensitivity with the value of 0.0000834 g/s/N/m. As a summary, each of parameter sensitivity have been identified and ranked accordingly.

Table 3. Parametric sensitivity ranking.

Ranking	Parametric Factor	Sensitivity Value	Unit
1	Nozzle Diameter (m)	1489.705	(g/s/m)
2	Armature Mass (kg)	337.667	(g/s/kg)
3	Injection Duration (s)	40.520	(g/s/s)
4	Input Voltage (V)	0.0844	(g/s/V)
5	Injection Pressure (bar)	0.0203	(g/s/bar)
6	Spring Constant (N/m)	0.0000834	(g/s/N/m)

5. Conclusion

A simulation model was built to recreate the experimental work that has been carried out to study the injection characteristics of CNG fuel on a single-hole direct injector. The simulation model can predict the mass flow rate of direct injector trendline but cannot detect the fluctuation in short injection duration. Some of the parameter will affect the mass flow rate of direct injector and some will have no effect on the mass flow rate. The most significant parameter affected the mass flow rate sensitivity was Nozzle Diameter followed by Armature Mass, Injection Duration, Input Voltage, Injection Pressure and Spring Constant. The results of the injection experiment and simulation are useful to understand the characteristics of the injector. Detail study of the inconsistency of injector mass flow rate is very crucial to help understanding the injection characteristics of the injector better. The simulation model of the injector able to predict the mass flow rate trend but were unable to spot the fluctuating trend. Further study on how to eliminate or reduce the fluctuating effect need to be done to ensure injector optimum performance.

Acknowledgement
The authors would like to thank to the Ministry of Higher Education (MOHE) and Universiti Malaysia Pahang for providing the funding for the project under grant scheme FRGS 2017-1 number RDU170127.

References

[1] H. Hao, Z. Liu, F. Zhao, and W. Li, "Natural gas as vehicle fuel in China : A review," vol. 62, pp. 521–533, 2016.
[2] S. Moon, "Potential of direct-injection for the improvement of homogeneous-charge combustion in spark-ignition natural gas engines," *Appl. Therm. Eng.*, vol. 136, no. January, pp. 41–48, 2018.
[3] T. Wang, X. Zhang, J. Zhang, and X. Hou, "Numerical analysis of the influence of the fuel injection timing and ignition position in a direct-injection natural gas engine," *Energy Convers. Manag.*, vol. 149, pp. 748–759, 2017.
[4] M. Baratta and N. Rapetto, "Mixture formation analysis in a direct-injection NG SI engine under different injection timings," *Fuel*, vol. 159, pp. 675–688, 2015.
[5] M. Choi, J. Song, and S. Park, "Modeling of the fuel injection and combustion process in a CNG direct injection engine," *Fuel*, vol. 179, pp. 168–178, 2016.
[6] Y. Liu, J. Yeom, and S. Chung, "A study of spray development and combustion propagation processes of spark-ignited direct injection (SIDI) compressed natural gas (CNG)," *Math. Comput. Model.*, vol. 57, no. 1, pp. 228–244, 2013.
[7] H. Muk and B. He, "Spark ignition natural gas engines — A review," vol. 48, pp. 608–618, 2007.
[8] H. Xu, C. Wang, X. Ma, A. K. Sarangi, A. Weall, and J. Krueger-venus, "Fuel injector deposits in direct-injection spark-ignition engines," *Prog. Energy Combust. Sci.*, vol. 50, pp. 63–80, 2015.
[9] W. Chen, J. Pan, B. Fan, Y. Liu, and O. Peter, "E ff ect of injection strategy on fuel-air mixing and combustion process in a direct injection diesel rotary engine (DI-DRE)," *Energy Convers. Manag.*, vol. 154, no. October, pp. 68–80, 2017.
[10] I. Erfan, I. Chitsaz, M. Ziabasharhagh, A. Hajialimohammadi, and B. Fleck, "Injection characteristics of gaseous jet injected by a single-hole nozzle direct injector," *Fuel*, vol. 160, pp. 24–34, 2015.
[11] M. A. Kalam and H. H. Masjuki, "An experimental investigation of high performance natural gas engine with direct injection," *Energy*, vol. 36, no. 5, pp. 3563–3571, 2011.
[12] P. H. Schimpf, "A Detailed Explanation of Solenoid Force," vol. 8, no. 2, 2013.
[13] W. B. Firmansyah, E. Z. Ayandotun, and A. Zainal, "Injection characteristics study of high-pressure direct injector for Compressed Natural Gas (CNG) using experimental and analytical method Injection characteristics study of high-pressure direct injector for Compressed Natural Gas (CNG) using experime," 2017.
[14] X. Zhang, A. Palazzolo, C. Kweon, E. Thomas, R. Tucker, and A. Kascak, "Direct Fuel Injector Power Drive System Optimization," vol. 7, no. 3, 2014.
[15] J. M. G. Antunes, "THE USE OF HYDROGEN AS A FUEL FOR," no. September, 2010.
[16] Z. T. and M. F. A. R. and R. Mamat, "Injection characteristics study of high-pressure direct injector for Compressed Natural Gas (CNG) using experimental and analytical method," *IOP Conf. Ser. Mater. Sci. Eng.*, vol. 257, no. 1, p. 12057, 2017.